Proceedings of ALGORITMY 2002
Conference on Scientific Computing, pp. 1–13

MULTISCALE SIMULATIONS OF INDUSTRIAL CRYSTAL GROWTH*

AXEL VOIGT, CHRISTIAN WEICHMANN† AND KARL-HEINZ HOFFMANN‡

Abstract. Crystal growth has been a focal point of intense applied research in resent years and significant progress has been made in many areas like growth techniques, process modeling and simulation, stresses in as-grown crystals, material characterization, defects and dislocations, process control and process design. It is widely accepted that today without an effective attendant process modeling no appropriate quality of the crystal can be achieved. Most approaches to model Czochralski crystal growth focus on heat and mass transfer on a macroskopic scale. Microscopic phenomena, indicating defects in the underlying lattice are mostly studies without any connection to the macroscopic growth process. The aim of this paper is the combination of macroscopic and microscopic phenomena in one model. The different length and time scales in Czochralski crystal growth lead to a hierarchy in the developed model. This hierarchy in combination with modern mathematical tools like residual based a posteriori error estimates and adaptive finite elements is used to efficiently solve the multiscale system. Experimental measurements proof the correctness of the simulation results. With this model a microscopic measure for crystal quality is related to macroscopic growth conditions.

Key words. heat transfer, defect diffusion, multiscale modeling, scientific computing

AMS subject classifications. 35K05, 35Q30, 45B05

1. Introduction. Czochralski growth is a complex process. The quality of the grown crystal depends on many macro- and microscopic effects. Macroscopically Czochralski growth in a simple form can be described as follows. There exist two different phases separated by a thin interface region. Processes at the interface transform one phase (melt) into the other (crystal), thereby displacing the position of the interface. The interface kinetics are controlled by the heat transport. The heat fluxes in the growth interface are driven by temperature gradients, which are needed to stabilize the melt-crystal interface. The heat flux tries to compensate the temperature differences between heat sources (heaters and latent heat) and heat sinks (walls of the furnace) to which heat is transported by conduction, radiation and convection. Crystallization proceeds because after a disturbance of equilibrium conditions e.g. by temperature change, it allows the supercooled melt to approach a new equilibrium composition. This releases latent heat and it is primarily the removal of the latent heat which controls the crystal pulling process. Because of the relatively low growth rates and the small supercooling crystals are grown essentially under thermodynamic equilibrium conditions. Since the melt-crystal interface happens to be an isotherm, a change in the interface profile implies variations in temperature gradients in the interface region and therefore influences the quality of the crystal.

To fabricate modern ICs, silicon crystals with a controlled oxygen concentration and a low concentration of microdefects are needed. In order to grow crystals meeting

* This work was partially supported by Wacker Siltronic Inc., the BMBF by grant no. 03HOM3CA and the DFG-Sonderforschungsbereich 611 Bonn, TP C5

†Crystal Growth group, research center caesar, Friedensplatz 16, 53111 Bonn, Germany (voigt@caesar.de, weichmann@caesar.de).

‡Modeling and Simulation group, research center caesar, Friedensplatz 16, 53111 Bonn, Germany (hoffmann@caesar.de).

these constraints a detailed understanding of the lattice structure in the growing crystal and the incorporation of atoms into the lattice at the melt-crystal interface is needed. Crystal growth proceeds at the interface by successive transfer of atoms which arrange themselves to generate unit cells of the crystal lattice one after another. One property affecting the speed at which atoms can be rearrange from one phase to the other is the mobility of the atoms in this region. At usual growth rates the attachment of one additional layer of unit cells to the crystal takes a relatively long time. Due to dynamical exchange rates of atoms between melt and crystal at the interface atomic layers are dissolved and regrown many times before a net gain of one lattice plane occurs.

Thermodynamic equilibrium conditions favor the formation of crystals with a certain concentration of lattice defects. The two fundamental point defects are the self-interstitial and the vacancy, which correspond to an excess silicon atom placed on an off-lattice site and a missing silicon lattice atom, respectively. These point defects can lead to a variety of larger more complex defects which can be divided into bulk dislocations (line-defects) and microdefects (three-dimensional agglomerates). It is generally agreed that the source of most observable microdefects is the condensation of supersaturated point defects. Point defects are incorporated into the crystal in their equilibrium concentrations and then diffuse and recombine rapidly in the high temperature portion of the crystal. Depending on the growth conditions, one of the defect species survives in excess. As the crystal cools it exceeds a critical supersaturation concentration and then leads to the formation of microdefects.

We present a model which relates the macroscopic growth conditions to the resulting microdefects in the growing crystal.

2. Mathematical model and numerical methods. The model is subdivided into three levels of detail. On the coarsest level the global heat transfer in a furnace is considered. Heat is primarily supplied to melt and crystal by radiation from nearby heaters. The calculated temperature field in melt and crystal is used on the second level to solve the free boundary problem, describing the crystallization together with an adequate melt flow approximation. On the finest level finally the temperature in the crystal is combined with the concentration of point-defects in the underlying crystal lattice.

2.1. Global heat transfer. The heat transfer in a Czochralski furnace is at the first approximation modeled by a nonlinear heat equation in all parts with radiating boundary conditions, Fig. 2.1.

$$\rho_{i_0} c_{i_p} \left(\frac{\partial T_i}{\partial t} + \mathbf{u}_i \cdot \nabla T_i \right) - \nabla \cdot (k_i \nabla T_i) = \rho_{i_0} h_i, \tag{2.1}$$

where ρ_{i_0} is the density of the component, c_{i_p} is the heat capacity, $\mathbf{u}_i$ is the velocity, including convection in the melt, rotation and lifting of the crucible as well as rotation and pulling of the crystal, k_i is the thermal conductivity and h_i is a heat source term. i indicates the different components of the apparatus, like crucible, heaters, heat shields and insulators. The heat source h_i is nonzero only in the heaters. The heating system is modeled by Ohmic resistors. The thermal dependence of electrical conductivity is dropped and the heat supply h_i is expressed as the product of the total power W and the power distribution in the resistors w.

We assume that almost no radiation is emitted or absorbed by the gas and that radiation is only diffuse. Moreover, we consider that emission, absorption and reflection of radiating waves occur only at the surfaces. By the Stefan-Boltzmann-Law the

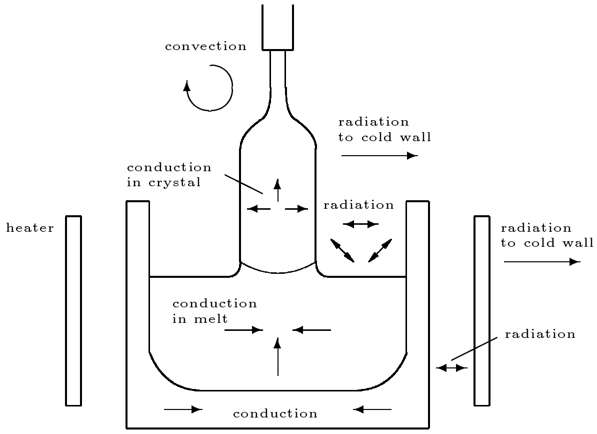

FIG. 2.1. *Schematic visualization of global heat exchange processes in a Czochralski furnace*

radiosity q_{total}, the total outgoing heat flux, is the sum of the surface emissive power and the reflected irradiation

$$q_{total} = \epsilon\gamma\sigma T^4 + (1-\epsilon)q_{in}. \tag{2.2}$$

The incident heat flux q_{in} is the sum of the contributions of the outgoing fluxes q_{total} from all other points on the surface. The irradiation on the surface is proportional to the radiation emitted by the different parts of the surface itself due to

$$q_{in}(\mathbf{r}) = \int_\Gamma \omega(\mathbf{r},\mathbf{s})\Xi(\mathbf{r},\mathbf{s})q_{total}(\mathbf{s})d\mathbf{s}, \tag{2.3}$$

where Γ is the surface being considering, $\mathbf{r},\mathbf{s} \in \Gamma$ and $\Xi(\mathbf{r},\mathbf{s})$ the visibility factor, which has a value 1 if the points $\mathbf{r}$ and $\mathbf{s}$ see each other, otherwise it has the value 0. The view factor $\omega(\mathbf{r},\mathbf{s})$ has the form

$$\omega(\mathbf{r},\mathbf{s}) = \frac{(\mathbf{n}_r \cdot (\mathbf{s}-\mathbf{r}))(\mathbf{n}_s \cdot (\mathbf{r}-\mathbf{s}))}{\pi\|\mathbf{s}-\mathbf{r}\|^4}, \tag{2.4}$$

where $\mathbf{n}_u$ and $\mathbf{n}_s$ are the surface normals directed to the gas phase. If one defines an operator

$$\mathbf{K}\lambda(\mathbf{r}) = \int_\Gamma \omega(\mathbf{r},\mathbf{s})\Xi(\mathbf{r},\mathbf{s})\lambda(\mathbf{s})d\mathbf{s},\ \forall r \in \Gamma, \tag{2.5}$$

one can write $q_{in} = \mathbf{K}q_{total}$ and from (2.2) one gets

$$q_{total} = (\mathbf{I} - (1-\epsilon)\mathbf{K})^{-1}\sigma\epsilon T^4. \tag{2.6}$$

The heat balance at the surface relating the heat flux caused by conduction to the surface q, the radiosity (2.2) and (2.6) and the irradiation (2.3) then becomes

$$q = \mathbf{G}(\sigma T^4), \tag{2.7}$$

where

$$\mathbf{G} = (\mathbf{I} - \mathbf{K})(\mathbf{I} - (1-\epsilon)\mathbf{K})^{-1}\epsilon \tag{2.8}$$

is the infinite dimensional equivalent of the so called Gebhart factors. Equation (2.7) serves as the boundary condition for (2.1) and couples the differential equations with the integral equation.

If one multiplies the heat equation (2.1) by a test function $\phi \in X(\Gamma_d, \Gamma_r, \Omega)$, with

$$X(\Gamma_1, \Gamma_2, \Omega) = \left\{\phi \in H_0^1(\Gamma_1, \Omega) \cap L^5(\Gamma_2)\right\}.$$

and integrates over the region $\Omega = \Omega_i$, uses Green's theorem and applies the radiation conditions at the gas boundary $\Gamma_r = \Gamma_{i/g}$ and the Dirichlet condition at the Dirchlet boundary $\Gamma_d = \Gamma_{i/j}$ one gets

$$\begin{aligned} \int_\Omega \rho_0 c_p \left(\frac{\partial T}{\partial t} + (\mathbf{u}_i \cdot \nabla T)\right) \phi d\Omega + \int_\Omega k \nabla T \cdot \nabla \phi d\Omega = \\ \int_\Omega \rho_0 h \phi d\Omega - \int_{\Gamma_r} q \phi dS, \end{aligned} \tag{2.9}$$

with $\rho_0 = \rho_{i_0}, c_p = c_{i_p}, k = k_i$ and $h = h_i$. For existence of a unique weak solution of (2.9) see Tiihonen [9]. The discretization of the heat transfer problem (2.9) combines piecewise linear finite elements in space and a time discretization including the convection that is based on the method of characteristics. The characteristic finite difference method is based on the approximation

$$\frac{\partial T(\mathbf{x},t)}{\partial t} + \mathbf{u}_i \cdot \nabla T(\mathbf{x},t) \approx \frac{T(\mathbf{x},t) - T(\mathbf{x} - \tau \mathbf{u}_i, t - \tau)}{\tau}. \tag{2.10}$$

The temperature is approximated as a linear combination of basis functions such that

$$T^{n+1} = \sum_{i=1}^{n} T_i^{n+1} \phi_i^{n+1}, \tag{2.11}$$

where $T_i^{n+1} \in I\!R$ and ϕ_i^{n+1} a piecewise linear nodal basis function of $X(\Gamma_d, \Gamma_r, \Omega)$. The discrete problem reads as follows: Given $T^n \in W^n$ find $T^{n+1} \in W^{n+1}$ such that for all $\phi^{n+1} \in W_{0_d}^{n+1}$

$$\begin{aligned} \frac{1}{\tau^n}\left(\rho_0 c_p \left(T^{n+1} - \bar{T}^n\right), \phi^{n+1}\right)_\Omega^{n+1} + \left(k \nabla T^{n+1}, \nabla \phi^{n+1}\right)_\Omega = \\ \left(\rho_0 h^{n+1}, \phi^{n+1}\right)_\Omega - \left(q^{n+1}, \phi^{n+1}\right)_{\Gamma_r}, \end{aligned} \tag{2.12}$$

with $\bar{T}^n(\mathbf{x}, t^n) = T^n(\mathbf{x} - \tau^n \mathbf{u}_i, t^n)$. The superscript $n+1$ at the scalar product indicates the interpolation onto the new grid before evaluation. In each time step equation (2.12) leads to the system of nonlinear algebraic equations

$$\mathbf{M}^T \mathbf{T}^{n+1} + \mathbf{A}^T \mathbf{T}^{n+1} = \mathbf{R}^T, \tag{2.13}$$

with the diagonal lumped mass matrix $\mathbf{M}^T = (M_{ii}^T)$,

$$M_{ii}^T = \frac{1}{\tau^n}(\rho_0 c_p \phi_i^{n+1}, \phi_i^{n+1})_\Omega, \tag{2.14}$$

the stiffness matrix $\mathbf{A}^T = (A_{ij}^T)$,

$$A_{ij}^T = (k \nabla \phi_i^{n+1}, \nabla \phi_j^{n+1})_\Omega \tag{2.15}$$

and the right hand side $\mathbf{R}^T = (R_i^T)$,

$$R_i^T = \frac{1}{\tau^n}(\rho_0 c_p \bar{T}^n, \phi_i^{n+1})_\Omega^{n+1} + (\rho_0 h^{n+1}, \phi_i^{n+1})_\Omega - (q^{n+1}, \phi_i^{n+1})_{\Gamma_r}. \tag{2.16}$$

Since the nonlinearities which are associated with temperature dependent material properties and boundary conditions in thermal diffusion problems are usually quite mild the method of succesive substitution is used in order to solve the nonlinear equation (2.13). This leads to the following algebraic equation for T_i^{n+1}

$$M_{ii}^T(T_i^m)T_i^{m+1} + \sum_j A_{ij}^T(T_j^m)T_j^{m+1} = R_i^T, \tag{2.17}$$

where superscripts indicate the iteration level, the timestep is not indicated for simplicity. The generalized minimum residual method (GMRES) is used for solving the linear system in each iteration.

The heat fluxes q^{n+1} in the radiation boundary conditions are related to the temperature at the surface, due to the Gebhard factor $\mathbf{G}$ defined in (2.8). A finite dimensional equivalent of $\mathbf{G}$ can be achieved by introducing the view factor

$$F_{ij} = \frac{1}{\|A_i\|}\int_{A_i}\int_{A_j} \frac{\mathbf{n}_i \cdot (\mathbf{x}_i - \mathbf{x}_j)\mathbf{n}_j \cdot (\mathbf{x}_i - \mathbf{x}_j)}{\pi\|\mathbf{x}_i - \mathbf{x}_j\|^4} \Xi(\mathbf{x}_i, \mathbf{x}_j) dA_i dA_j, \tag{2.18}$$

and replacing the integral operator $\mathbf{K}$ in (2.5) with (2.18). A_i and A_j represent the element surface areas with $\mathbf{x}_i \in A_i, \mathbf{x}_j \in A_j$, $\mathbf{n}_i$ and $\mathbf{n}_j$ the corresponding outward unit normals and $\Xi(\mathbf{x}_i, \mathbf{x}_j)$ the visibility factor. The discrete version of $\mathbf{G}$ can now be defined by $\mathbf{G}^{n+1} = (\mathbf{I} - \mathbf{F})(\mathbf{I} - (\mathbf{I} - \mathbf{E})\mathbf{F})^{-1}\mathbf{E}$ with $\mathbf{E}$ a diagonal matrix containing the surface emissivities. An energy balance for each surface leads to the following system of equations

$$\sum_{j=1}^{n} (\delta_{ij} - (1 - \epsilon_i) F_{ij}) q_{total_j}^{n+1} = \epsilon_i \sigma T (H_i^{n+1})^4 \tag{2.19}$$

and

$$q_i^{n+1} = q_{total_i}^{n+1} - \sum_{j=1}^{n} F_{ij} q_{total_j}^{n+1}, \tag{2.20}$$

where it is assumed that the surface is decomposed into n disjoint subsets A_i. When the surface temperatures for all surfaces are known, equation (2.19) forms a set of linear algebraic equations for the unknown, total outgoing heat flux, $\mathbf{q}_{total}^{n+1}$. That is, equation (2.19) can be written as

$$\mathbf{P}\mathbf{q}_{total}^{n+1} = \mathbf{Q}, \tag{2.21}$$

with the matrix $\mathbf{P} = (P_{ij})$,

$$P_{ij} = \delta_{ij} - (1 - \epsilon_i) F_{ij}, \tag{2.22}$$

and the vector $\mathbf{Q} = (Q_i)$,

$$Q_i = \epsilon_i \sigma T_i^4. \tag{2.23}$$

When the $\mathbf{q}_{total}^{n+1}$ values are available, equation (2.20) is then used to compute the effective flux to the surface $\mathbf{q}^{n+1}$ with provides the boundary condition to the finite element model for the conduction process. The surface temperatures used in the above computation must be uniform over each surface in order to satisfy the condition of the radiation model. It is assumed that each surface in the radiation problem corresponds to a face or edge of a finite element. The uniform surface temperature can be obtained by averaging the nodal point temperatures on the appropriate element face or edge.

The matrix $\mathbf{P}$ is a full matrix due to the surface to surface coupling represented by the view factors F_{ij}. The method of successive overrelaxation is used for solving the algebraic system. A more advanced way to calculate the view factors is described in Voigt et al. [12].

2.2. Melt-crystal system. The computed temperatures and heat fluxes at the boundary of the crystal and melt are now used as boundary conditions for a more detailed model of heat transfer including the free crystallization interface and the influence of convection in the melt, Fig. 2.2.

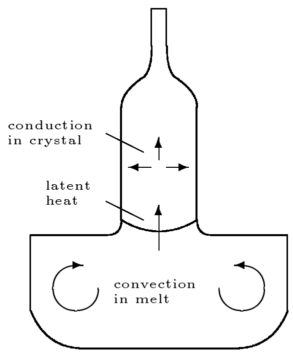

FIG. 2.2. *Free boundary problem in local melt-crystal system*

Instead of formulating the problem with the help of the heat equation (2.1) in melt and crystal and Stefan-boundary condition an equation for enthalpy H can be introduced and enthalpy can be treated as the primary unknown. The energy density (or enthalpy) H is defined as:

$$H(T) = \int_{T_{ref}}^{T} \rho c(\tau) d\tau + l\eta\,(T - T_{eq}) \tag{2.24}$$

with

$$\eta(\delta) = \begin{cases} 1 & , \quad \delta \geq 0 \\ 0 & , \quad \delta < 0. \end{cases} \tag{2.25}$$

By applying a Kirchhoff transformation

$$\alpha(T) = \int_{T_{ref}}^{T} k(\tau) d\tau \tag{2.26}$$

one can simplify the nonlinear heat equations (2.1). One has $k_i \nabla T = \nabla \alpha(T)$ and therefore the heat equation (2.1) take the simpler form $\rho_{i_0} c_{i_p} \left(\frac{\partial T_i}{\partial t} + \mathbf{u}_i \cdot \nabla T_i \right) -$

$\Delta\alpha(T_i) = 0$. Instead of defining enthalpy as a function of temperature one can define temperature as the inverse of (2.24) and again apply a Kirchhoff transformation to get $\beta(H)$ which in the simplified case of piecewise constant physical coefficients can be written as

$$\beta(H) = \begin{cases} \frac{k_c}{\rho_c c_{p_c}} H & , \quad H < \rho_c c_{p_c} T_{eq} \\ k_c T_{eq} & , \quad H \in [\rho_c c_{p_c} T_{eq}, \rho_c c_{p_c} T_{eq} + \rho_c l] \\ \frac{k_m (H - \rho_c l - \rho_c c_{p_c} T_{eq})}{\rho_m c_{p_m}} + k_c T_{eq} & , \quad H > \rho_c c_{p_c} T_{eq} + \rho_c l \end{cases} \tag{2.27}$$

Now the equation (2.1) can be written as

$$\frac{\partial H}{\partial t} + \mathbf{u}_i \cdot \nabla H - \Delta\beta(H) = 0 \tag{2.28}$$

in $\Omega_m \cup \Omega_c$. Instead of a two region problem with a jump condition one now has a one region problem with rapidly varying coefficients. This formulation does not explicitly include the position of the interface. The interface is given implicitly by the melting temperature isotherm. The enthalpy formulation seeks to reconsider the thermodynamic assumptions upon which the Stefan problem is based and sidesteps the necessity to track the interface. Equation (2.28) holds only in the weak sense. If one multiplies (2.28) by a test function $\phi \in X(\Gamma_d, \Gamma_r, \Omega)$, integrates over the region $\Omega = \Omega_m \cup \Omega_c$, uses Green's theorem and applies the radiation conditions at the melt-gas and crystal-gas boundary $\Gamma_r = \Gamma_{m/g} \cup \Gamma_{c/g}$ and the Dirichlet condition at the melt-crucible boundary $\Gamma_d = \Gamma_{m/cr}$ one gets

$$\int_\Omega \left(\frac{\partial H}{\partial t} + (\mathbf{u}_i \cdot \nabla H) \right) \phi d\Omega + \int_\Omega \nabla\beta(H) \cdot \nabla\phi d\Omega = -\int_{\Gamma_r} q\phi dS. \tag{2.29}$$

Existence of a unique weak solution of (2.29) is known for the problem without convection, see Visintin [10] for the problem without radiation and Metzger [6] for the problem with radiation.

The full discretization of the phase transition problem (2.28) combines piecewise linear finite elements in space and a time discretization including the convection that is based on the method of characteristics. The characteristic finite difference method is based on the approximation

$$\frac{\partial H(\mathbf{x}, t)}{\partial t} + \mathbf{u}_i \cdot \nabla H(\mathbf{x}, t) \approx \frac{H(\mathbf{x}, t) - H(\mathbf{x} - \tau\mathbf{u}_i, t - \tau)}{\tau}. \tag{2.30}$$

Because $H(\mathbf{x} - \tau\mathbf{u}_i, t - \tau)$ is well defined only for $\mathbf{x} - \tau\mathbf{u}_i \in \bar{\Omega}$ the time step size τ has to be restricted locally. Enthalpy and temperature are approximated as linear combinations of basis functions such that

$$H^{n+1} = \sum_{i=1}^{n} H_i^{n+1} \phi_i^{n+1}, \quad \Theta^{n+1} = \beta(H^{n+1}), \tag{2.31}$$

where $H_i^{n+1} \in I\!R$ and ϕ_i^{n+1} a piecewise linear nodal basis function of $X(\Gamma_d, \Gamma_r, \Omega)$. The discrete problem reads as follows:

$$\frac{1}{\tau^n} \left(H^{n+1} - \bar{H}^n, \phi^{n+1} \right)_\Omega^{n+1} + \left(\nabla\Theta^{n+1}, \nabla\phi^{n+1} \right)_\Omega = -\left(q^{n+1}, \phi^{n+1} \right)_{\Gamma_r}, \tag{2.32}$$

with $\bar{H}^n(\mathbf{x}, t^n) = H^n(\mathbf{x} - \tau^n \mathbf{u}_i, t^n)$. In each time step equation (2.32) leads to the system of nonlinear algebraic equations

$$\mathbf{M}^H \mathbf{H}^{n+1} + \mathbf{A}^H \boldsymbol{\Theta}^{n+1} = \mathbf{R}^H, \tag{2.33}$$

with the diagonal lumped mass matrix $\mathbf{M}^H = (M_{ii}^H)$,

$$M_{ii}^H = \frac{1}{\tau^n}(\phi_i^{n+1}, \phi_i^{n+1})_\Omega, \tag{2.34}$$

the stiffness matrix $\mathbf{A}^H = (A_{ij}^H)$,

$$A_{ij}^H = (\nabla \phi_i^{n+1}, \nabla \phi_j^{n+1})_\Omega \tag{2.35}$$

and the right hand side $\mathbf{R}^H = (R_i^H)$,

$$R_i^H = \frac{1}{\tau^n}(\bar{H}^n, \phi_i^{n+1})_\Omega^{n+1} - (q^{n+1}, \phi_i^{n+1})_{\Gamma_r}. \tag{2.36}$$

The system (2.33) leads to the following algebraic equation for H_i^{n+1}

$$M_{ii}^H H_i^{n+1} + A_{ii}^H \Theta_i^{n+1} = R_i^H - \sum_{j \neq i} A_{ij}^H \Theta_j^{n+1}, \quad \Theta_i^{n+1} = \beta(H_i^{n+1}). \tag{2.37}$$

The method of successive overrelaxation is used for solving the algebraic system.

2.3. Defect distribution. The free phase boundary as well as the temperature distribution in the crystal now serves as input for the defect model. The presence of point defects in the lattice is due to thermal vibrations of the silicon atoms at finite temperatures. For a detailed discussion of intrinsic point defect diffusion in silicon, we refer to [3]. In a continuum approach we describe diffusion fluxes of atomic species that are driven by the gradient of the chemical potential, which is a function of temperature, pressure and the concentration distribution of the diffusion species. Diffusion of point defect species due to concentration and temperature gradients are governed by Fickian and thermal diffusion laws. Pressure gradients occur in cooling crystals in the form of thermal stresses.

Self-interstitials and vacancies are incorporated into the crystal in their equilibrium concentrations and then diffuse and recombine rapidly in the high temperature portion of the crystal. Depending on the growth conditions, one of these defect species survives in excess and leads to the formation of the corresponding microdefects, Fig. 2.3.

The conservation equations for intrinsic point defects include convective, Fickian diffusion, thermal diffusion and recombination terms. The equations can be derived from basic principles of thermodynamic, see [1]. The governing equations for the concentrations of interstitials and vacancies are

$$\frac{\partial C_i}{\partial t} + \mathbf{u}_c \cdot \nabla C_i - \nabla \cdot \left(D_i \nabla C_i - \frac{Q_i D_i C_i}{k T_c^2} \nabla T_c \right) = k_{rec} \left(C_i^{eq} C_v^{eq} - C_i C_v \right), \tag{2.38}$$

$$\frac{\partial C_v}{\partial t} + \mathbf{u}_c \cdot \nabla C_v - \nabla \cdot \left(D_v \nabla C_v - \frac{Q_v D_v C_v}{k T_c^2} \nabla T_c \right) = k_{rec} \left(C_i^{eq} C_v^{eq} - C_i C_v \right), \tag{2.39}$$

where C_i and C_v are the concentrations of interstitials and vacancies, D_i and D_v the diffusion coefficients, Q_i and Q_v the activation enthalpy for thermal diffusion, C_i^{eq} and

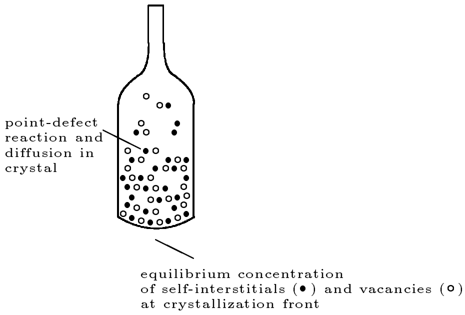

FIG. 2.3. *Reaction and diffusion processes in crystal*

C_v^{eq} the equilibrium concentrations, T temperature, $\mathbf{u_c}$ the velocity of the crystal, k the Boltzmann constant and k_{rec} the reaction coefficient for recombination. Convection of self-interstitials and vacancies occurs as bulk transport. Fickian diffusion is driven by concentration gradients. The flux of the diffusing species $J = -D\nabla C$ is in the direction of lower concentrations. The diffusion coefficient D depends on temperature and concentration. Due to the low concentrations of intrinsic point defects, $10^{-16}cm^{-3}$, the concentration dependence is neglected. Thermal diffusion is driven by temperature gradients in the direction of higher temperature and the flux is proportional to its activation energy Q, the diffusion coefficient D and the temperature T. Recombination is identical for both species and describes the elimination of self-interstitials and vacancies by the creation of perfect lattice sites. The low concentrations of point defects show no influence on the temperature distribution in the crystal. A coupling of both phenomena exists therefore only because of the temperature dependent material properties of the defects, see also Voigt et al. [13].

If one multiplies the reaction-diffusion equation (2.39) by a test function $\phi \in H_0^1(\Gamma, \Omega)$, integrates over the region $\Omega = \Omega_c$, uses Green's theorem and applies the Dirichlet conditions at the boundary $\Gamma = \Gamma_{c/g} \cup \Gamma_{c/m}$ one gets

$$\begin{aligned} &\int_\Omega \left(\frac{\partial C}{\partial t} + (\mathbf{u}_c \cdot \nabla C) \right) \phi d\Omega + \int_\Omega D \nabla C \cdot \nabla \phi d\Omega - \\ &\int_\Omega \frac{QDC}{kT^2} \nabla T \cdot \nabla \phi d\Omega = \int_\Omega k_{rec} \left(C_i^{eq} C_v^{eq} - C_i C_v \right) \phi d\Omega, \end{aligned} \tag{2.40}$$

where $C = C_i$ or C_v, $D = D_i$ or D_v and $Q = Q_i$ or Q_v. For existance of a unique weak solution of (2.40) see Lang [5]. The discretization of the reaction-diffusion problem (2.40) combines piecewise linear finite elements in space and a time discretization including the convection that is based on the method of characteristics. The characteristic finite difference method is based on the approximation

$$\frac{\partial C(\mathbf{x},t)}{\partial t} + \mathbf{u}_c \cdot \nabla C(\mathbf{x},t) \approx \frac{C(\mathbf{x},t) - C(\mathbf{x} - \tau \mathbf{u}_c, t - \tau)}{\tau}. \tag{2.41}$$

The concentrations are approximated as a linear combination of basis functions such that

$$C^{n+1} = \sum_{i=1}^{n} C_i^{n+1} \phi_i^{n+1}, \tag{2.42}$$

where $C_i^{n+1} \in I\!R$ and ϕ_i^{n+1} a piecewise linear nodal basis function of $H_0^1(\Gamma, \Omega)$. The discrete problem reads as follows: Given $C^n \in W^n$ find $C^{n+1} \in W^{n+1}$ such that for all $\phi^{n+1} \in W_{0_d}^{n+1}$

$$\begin{aligned} &\frac{1}{\tau^n}\left(C^{n+1} - \bar{C}^n, \phi^{n+1}\right)_\Omega^{n+1} + \left(D\nabla C^{n+1}, \nabla\phi^{n+1}\right)_\Omega - \\ &\left(\frac{QDC^{n+1}}{kT^2}\nabla T, \nabla\phi^{n+1}\right)_\Omega = \left(k_{rec}\left(C_i^{eq}C_v^{eq} - C_i^{n+1}C_v^{n+1}\right), \phi^{n+1}\right)_\Omega, \end{aligned} \tag{2.43}$$

with $\bar{C}^n(\mathbf{x}, t^n) = C^n(\mathbf{x} - \tau^n \mathbf{u}_c, t^n)$. In each time step equation (2.43) leads to a system of nonlinear algebraic equations

$$\mathbf{M}^C\mathbf{C}_i^{n+1} + \mathbf{A}^{C_i}\mathbf{C}_i^{n+1} + \mathbf{B}^{C_i}\mathbf{C}_i^{n+1} + \mathbf{C}^{C_i}\mathbf{C}_i^{n+1} = \mathbf{R}^{C_i}, \tag{2.44}$$

$$\mathbf{M}^C\mathbf{C}_v^{n+1} + \mathbf{A}^{C_v}\mathbf{C}_v^{n+1} + \mathbf{B}^{C_v}\mathbf{C}_v^{n+1} + \mathbf{C}^{C_i}\mathbf{C}_v^{n+1} = \mathbf{R}^{C_v}, \tag{2.45}$$

with the diagonal lumped mass matrix $\mathbf{M}^C = (M_{ii}^C)$,

$$M_{ii}^C = \frac{1}{\tau^n}(\phi_i^{n+1}, \phi_i^{n+1})_\Omega, \tag{2.46}$$

the stiffness matrices $\mathbf{A}^{C_i} = (A_{ij}^{C_i})$ and $\mathbf{A}^{C_v} = (A_{ij}^{C_v})$,

$$A_{ij}^{C_i} = (D_i\nabla\phi_i^{n+1}, \nabla\phi_j^{n+1})_\Omega, \tag{2.47}$$

$$A_{ij}^{C_v} = (D_v\nabla\phi_i^{n+1}, \nabla\phi_j^{n+1})_\Omega, \tag{2.48}$$

the gradient matrices $\mathbf{B}^{C_i} = (B_{ij}^{C_i})$ and $\mathbf{B}^{C_v} = (B_{ij}^{C_v})$,

$$B_{ij}^{C_i} = (\frac{Q_iD_i}{kT^2}\nabla T\phi_i^{n+1}, \nabla\phi_j^{n+1})_\Omega, \tag{2.49}$$

$$B_{ij}^{C_v} = (\frac{Q_vD_v}{kT^2}\nabla T\phi_i^{n+1}, \nabla\phi_j^{n+1})_\Omega, \tag{2.50}$$

the recombination matrices $\mathbf{C}^{C_i} = (C_{ij}^{C_i})$ and $\mathbf{C}^{C_v} = (C_{ij}^{C_v})$,

$$C_{ij}^{C_i} = (k_{rec}C_v\phi_i^{n+1}, \phi_j^{n+1})_\Omega, \tag{2.51}$$

$$C_{ij}^{C_v} = (k_{rec}C_i\phi_i^{n+1}, \phi_j^{n+1})_\Omega, \tag{2.52}$$

and the right hand sides $\mathbf{R}^{C_i} = (R_{ij}^{C_i})$ and $\mathbf{R}^{C_v} = (R_{ij}^{C_v})$,

$$R_i^{C_i} = \frac{1}{\tau^n}(\bar{C}_i^n, \phi_i^{n+1})_\Omega^{n+1} + (k_{rec}C_i^{eq}C_v^{eq}, \phi_i^{n+1})_\Omega \tag{2.53}$$

$$R_i^{C_v} = \frac{1}{\tau^n}(\bar{C}_v^n, \phi_i^{n+1})_\Omega^{n+1} + (k_{rec}C_i^{eq}C_v^{eq}, \phi_i^{n+1})_\Omega. \tag{2.54}$$

Because of the nonlinearity in the recombination terms a Newton method is used to solve the nonlinear system (2.45). The generalized minimum residual method (GMRES) is used for solving the linear system in each iteration.

2.4. Coupling of equations. The overall numerical method is based on a semi implicit time discretization scheme with a coupling of the subproblems of global heat transfer, local phase transition and defect evolution. Because of the different time and length scales in the subproblems the system can be decoupled in the described way. Due to the axisymmetry of the furnace the complexity of the problem can be reduced to 2D. An unstructured triangular mesh is used for the discretisation. The software CrysVUN [4] and ALBERT [7] are used for the computations. For quasi-static simulations, taking not into account the growing of the crystal, the model was verified on experimental measurements, see Voigt et al. [11]. This simulation results confirmed qualitatively Voronkov's v/G theory, [14]. In the new transient model the growth process is solved for constant pulling velocities. Due to the change in the geometry resulting from the growing of the crystal, the grid is remeshed in each time step.

3. Numerical results. The simulations are performed for an experimental furnace to grow crystals with 200mm diameter. In the same hot zone three different pull rates where used, $v_{p1} = 0,348$mm/min, $v_{p2} = 0,454$mm/min and $v_{p3} = 0,892$mm/min, to simulate the growing process over a time interval of 250min. All simulations start with an initial quasi steady state computation for a crystal length of $10cm$. We only show the resulting temperature and defect distribution in the crystal.

3.1. Temperature profile. The computed temperature distributions in the crystal agree well with experiences from temperature measurements, Seidl et al. [8].

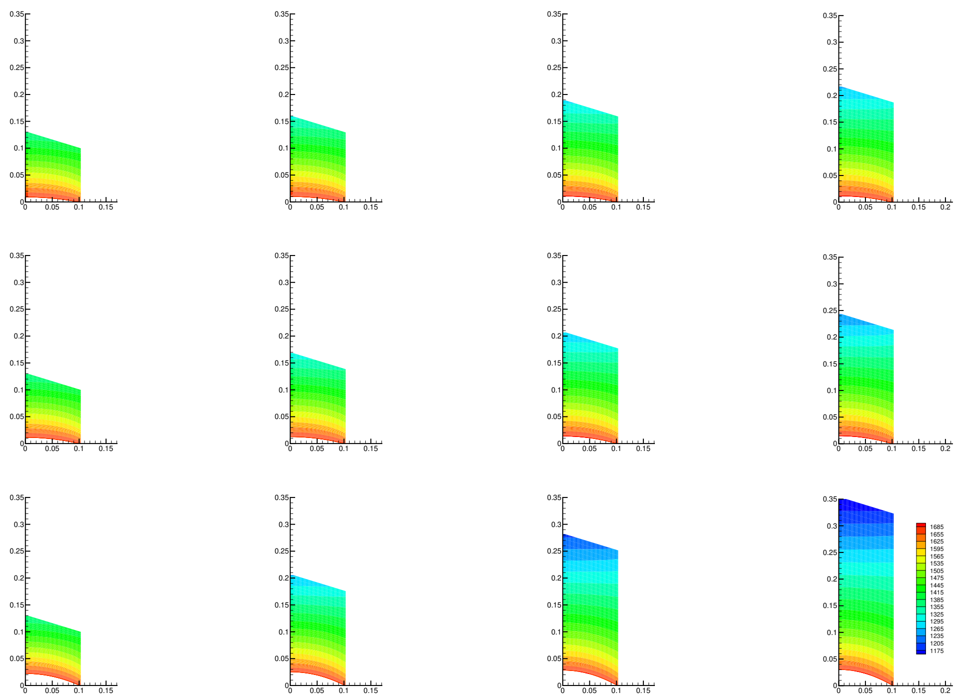

FIG. 3.1. *Temperature profile for pulling velocities v_{p1}, v_{p2} and v_{p3} and time steps $1 = 0min, 2 = 85min, 3 = 170min$ and $4 = 250min$.*

The upper part of the crystal continuously cools down during the growth process.

The axial temperature gradient is larger close to the phase boundary and decreases with increasing crystal length. The calculations clearly show that the shape of the phase boundary depends on the crystal length, Fig. 3.1. Under the same growth conditions, the phase boundary is more deflected for longer crystals. This is due to higher temperatures inside the crystal resulting from a lower surface to volume ratio for longer crystals which reduces the release of latent heat at the surface.

3.2. Defect distribution. At the interface, interstitials and vacancies are incorporated at their equilibrium concentration of 1.0e-15 and 1.2e-15cm^{-3}, respectively. Fast recombination in the high temperature part of the crystal reduces both concentrations. At a temperature of approximately 1200K, axial point defect concentrations become stable. Fully coupled transient heat and transient point defect simulations are performed. Highest interstitial concentrations occur in the crystal which is grown with the lowest pull rate v_{p1}. This crystal is fully interstitial-rich after cooling down. The crystal grown with pull rate v_{p2} shows vacancy-rich as well as interstitial-rich regions and the crystal grown with pull rate v_{p3} is completely vacancy-rich after cooling down. Fig. 3.2 shows normalized differences between the concentration of interstitials and vacancies. Positive (red) values indicate an excess of interstitials, negative (blue) values an excess of vacancies.

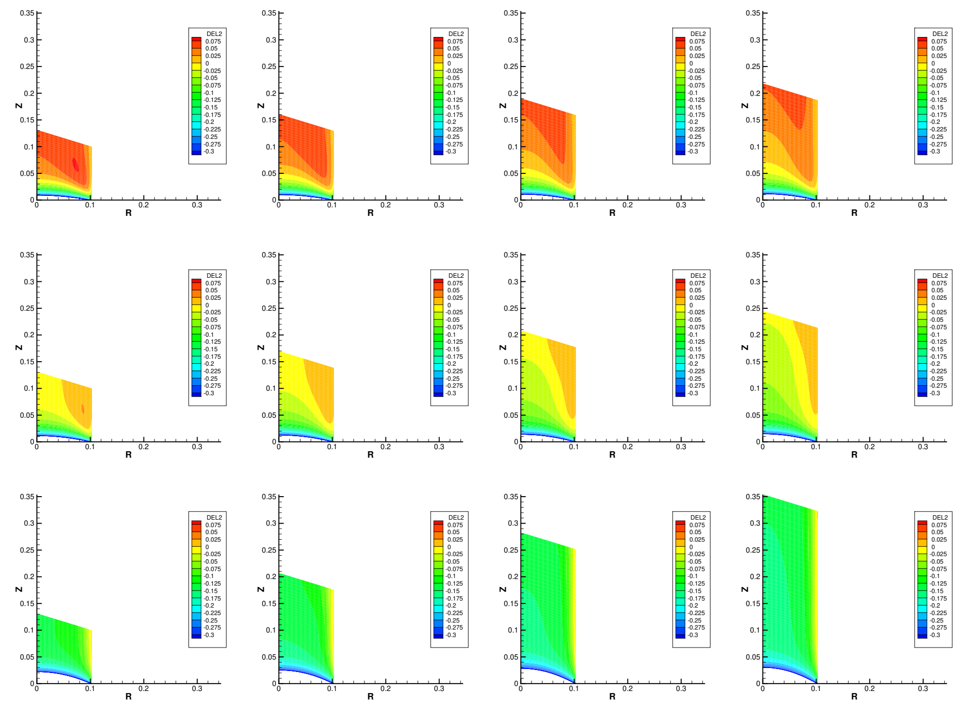

FIG. 3.2. *Defect concentration for pulling velocities v_{p1}, v_{p2} and v_{p3} and time steps $1 = 0min, 2 = 85min, 3 = 170min$ and $4 = 250min$, a normed difference between C_i and C_v is shown.*

REFERENCES

[1] S. R. de Groot and P. Mazur, *Non-equilibrium Thermodynamics*, North-Holland, Amsterdam, 1984

[2] E. Dornberger, *Prediction of OSF Ring Dynamics and Grown-in Voids in Czochralski Silicon Crystals*, PhD Thesis, Universite Catholique de Louvain, 1997

[3] P. Fahey, P. Griffin, J. Plummer, *Point defects and dopant diffusion in silicon*, Rev. Modern Physics, 61 (1989) pp. 291–306

[4] M. R. H. Kurz, *Development of CrysVUN++, a Software System for Numerical Modelling and Control of Industrial Crystal Growth Processes*, PhD Thesis, Universität Erlangen-Nürnberg, 1998

[5] J. Lang, *Adaptive Multilevel Solution of Nonlinear Parabolic PDE Systems*, Springer, Berlin, 2001

[6] M. Metzger, *Existence for a time-dependent heat equation with nonlocal radiation terms*, Math. Meth. Appl. Sci., 22, (1999) pp. 1101–1119

[7] A. Schmidt, K. G. Siebert *ALBERT: An adaptive hierarchical finite element toolbox.* Math. Tech. Report., Uni. Freiburg 6/2000

[8] A. Seidl, G. Müller, E. Dornberger, E. Tomzig, B. Rexer, W. von Ammon, Electrochem. Soc. Proc. 98-1 (1998), pp. 417–.

[9] T. Tiihonen, J. Järvinen, R. Nieminen, *Time-dependent simulation of Czochralski silicon crystal growth*, J. Cryst. Growth, 180 (1997), pp. 468–476

[10] A. Visintin, *Models of Phase Transition*, Birkhäuser, Bosten, 1996

[11] A. Voigt and J. Nitschkowski and C. Weichmann and K.-H. Hoffmann, *Controlling Point Defects in Single Silicon Crystals Grown by the Czochralski Method*, Lect. Notes Comp. Sci. Eng., 21 (2002), pp. 229–236.

[12] A. Voigt and N. Hanssen and C. Weichmann, *The radiosity equation for solving global heat transfer in industrial furnaces*, caesar-preprint, 21/2002

[13] A. Voigt and C. Weichmann, *Transport of point defects in growing Si crystals*, submitted

[14] V. Voronkow *The mechanism of swirl defects formation in silicon*, J. Cryst. Growth, 59 (1982), pp. 625–643